



HAL
open science

Tetrameric Lanthanide-Substituted Silicotungstate Ln 8 Si 4 W 40 Nanoclusters: Synthesis, Structural Characterization, Electrochemistry, and Catalytic Application for Oxidation of Thioethers

Imran Khan, Vivek Das, Anne-Lucie Teillout, I.M. Mbomekalle, Pedro de
Oliveira, Subash Chandra Sahoo, Firasat Hussain

► **To cite this version:**

Imran Khan, Vivek Das, Anne-Lucie Teillout, I.M. Mbomekalle, Pedro de Oliveira, et al.. Tetrameric Lanthanide-Substituted Silicotungstate Ln 8 Si 4 W 40 Nanoclusters: Synthesis, Structural Characterization, Electrochemistry, and Catalytic Application for Oxidation of Thioethers. *European Journal of Inorganic Chemistry*, 2021, 2021 (11), pp.1071-1081. 10.1002/ejic.202001096 . hal-03450093

HAL Id: hal-03450093

<https://hal.science/hal-03450093>

Submitted on 26 Nov 2021

HAL is a multi-disciplinary open access archive for the deposit and dissemination of scientific research documents, whether they are published or not. The documents may come from teaching and research institutions in France or abroad, or from public or private research centers.

L'archive ouverte pluridisciplinaire **HAL**, est destinée au dépôt et à la diffusion de documents scientifiques de niveau recherche, publiés ou non, émanant des établissements d'enseignement et de recherche français ou étrangers, des laboratoires publics ou privés.

Tetrameric Lanthanide-Substituted Silicotungstate $\{Ln_8Si_4W_{40}\}$ Nanoclusters: Syntheses, Structural Characterization, Electrochemistry and Catalytic Application for Oxidation of Thioethers

Imran Khan,^[a] Vivek Das,^[a] Anne-Lucie Teillout,^[b] Israël-Martyr Mbomekallé,^[b] Pedro de Oliveira,^[b] Subash Chandra Sahoo,^[c] and Firasat Hussain*^[a]

Dedication ((optional))

- [a] Mr. Imran Khan, Mr. Vivek Das, Dr. Firasat Hussain*
Department of Chemistry
University of Delhi, Faculty of Science, North Campus, Delhi-110007, India
E-mail: fhussain@chemistry.du.ac.in
- [b] Ms. Anne-Lucie Teillout, Dr. Israël-Martyr Mbomekallé, Prof. Pedro de Oliveira
Institut de Chimie Physique, UMR 8000 CNRS, Bâtiment 350, Faculté des Sciences d'Orsay,
Université Paris-Saclay, 91405 Orsay Cedex – France
- [c] Dr. Subash Chandra Sahoo
Department of Chemistry & Center of Advanced Studies in Chemistry
Panjab University, Chandigarh-160014, India.

Supporting information for this article is given via a link at the end of the document.

Abstract: All the title nanoclusters **1-10** with the molecular formula $[(Ln_8SiW_{10}O_{38})(W_3O_8)(OH)_4(H_2O)_2]^{26-}$ [$Ln^{III} = Sm$ (**1**), Eu (**2**), Gd (**3**), Tb (**4**), Dy (**5**), Ho (**6**), Er (**7**), Tm (**8**), Yb (**9**), and Y (**10**)] have been synthesized and isolated as mixed sodium and potassium salts. These nanoclusters are characterized by various analytical techniques such as FT-IR, UV/Vis, Photoluminescence, Single crystal X-ray diffraction, Electrochemistry, ICP-AES and Thermogravimetric analysis, and Powder X-ray diffraction. The $\{Ln_8Si_4W_{40}\}$ complexes show high efficiency and selectivity for the oxidation of thioethers using H_2O_2 as green oxidant. It is worth mentioning that the catalyst can be recovered even after five cycles of reaction with only a slight loss in its activity.

Introduction

Polyoxometalates (POMs) are metal-oxygen nanoclusters that consist of early transition metals such as Mo (VI), W (VI), and V (V) in their highest oxidation state. Due to the flexibility in their structure, size, charge density, and redox potential, POMs show various interesting applications in many fields like medicine, material science, catalysis, magnetism, clinical chemistry, photochemistry, and analytical chemistry.^[1-8] The lacunary POMs can be derived from their parent compounds such as Keggin-type ions $[XW_{12}O_{40}]^{n-}$ ($X = As^V, P^V, Ge^IV, Si^IV$, etc.), and these lacunary POMs consist of multiple oxygen donor atoms as well as multiple coordination sites which are more susceptible to construct a variety of structures. It is known that lanthanide-containing POMs exhibit structural varieties and have impressive properties that are useful in various application fields as mentioned above. A wide range of research papers has been published on lanthanide-substituted lacunary POMs. In the year 1971, Peacock and Weakley reported the synthesis of the first lanthanide-containing polyoxometalates. However, structural characterization evidence was not provided.^[9] Pope and co-workers reported a cerium-containing arsenotungstate of

molecular formula $[Ce_{16}As_2(H_2O)_{36}W_{148}O_{524}]^{76-}$.^[10] In 1991, Qu *et al.* reported the interaction of a monolacunary Keggin-type silicotungstate with early lanthanide ions to form $[Ln(\beta-SiW_{11}O_{39})]^{13-}$ polyanions ($Ln^{III} = La, Ce, Pr, Nd, Sm, Gd$, and Er). However, no structural evidence was provided either.^[11] Mialane *et al.* synthesized the lanthanide-substituted monolacunary Keggin-type silicotungstate polyanions $[Ln(\alpha-SiW_{11}O_{39})]^{8-}$ ($Ln^{III} = Yb, Nd, Eu$, and Gd). They found that these isolated compounds were strongly affected by the nature of the lanthanide cations.^[12] Gouzerh *et al.* in 2002, reported a cerium-containing antimonate $[Ce_3Sb_4W_2O_8(H_2O)_{10}(SbW_9O_{33})_4]^{19-}$ and arsenotungstate $[Ce(H_2O)_5As_4W_{40}O_{140}]^{25-}$.^[13] Niu *et al.* reported a one-dimensional (1D) structure with the formula $K_3[(Pr(H_2O)_4SiW_{11}O_{39})(NaPr_2(H_2O)_{12})(Pr(H_2O)_4SiW_{11}O_{39}) \cdot 13.5H_2O]$.^[14] The crystal structure of this complex consists of two distinct units of $[Pr(H_2O)_4SiW_{11}O_{39}]^{5-}$ and one $[NaPr_2(H_2O)_{12}]^{7+}$ subunit, that is further linked with the help of praseodymium and sodium cations via bridging and terminal oxygen atoms of the Keggin ion $[\alpha-SiW_{11}O_{39}]^{8-}$, giving rise to a complete one-dimensional structure. In 2006, Niu *et al.* also synthesized 1D and 2D structures of three new organic-inorganic hybrid monolacunary Keggin-type silico and germanotungstate of the formula $H\{[Sm(H_2O)_{5.5}(DMF)_{0.5}]_2[Sm(H_2O)_2(DMF)]\{[Sm(H_2O)_3(\alpha-SiW_{11}O_{39})]_2\}, [Sm(H_2O)_6]_{0.25}[Sm(H_2O)_5]_{0.25}H_{0.5}\{[Sm(H_2O)_7-Sm(H_2O)_2(DMSO)(\alpha-SiW_{11}O_{39})] \cdot 45H_2O, and [Dy(H_2O)_4]_{0.25}[Dy(H_2O)_6]_{0.25}H_{0.5}\{[Dy(H_2O)_7][Dy(H_2O)_2(DMSO)(\alpha-GeW_{11}O_{39})] \cdot 25H_2O}$.^[15] All three compounds show good thermal stability and magnetic properties. In 2007, Kortz *et al.* have reported twenty cerium-containing germanotungstates of the formula $[Ce_{20}Ge_{10}W_{100}O_{376}(OH)_4(H_2O)_{36}]^{56-}$.^[16] Patzke *et al.* isolated three new lanthanide-substituted silicotungstates based on open Wells-Dawson fragments $[Ln_2(H_2O)_7SiW_{18}O_{66}]^{10-}$ ($Ln^{III} = Eu$, and Tb) and a sandwich-type monolacunary Keggin-type $[Eu(\alpha-SiW_{11}O_{39})_2]^{13-}$ polyanion.^[17] In 2008, Khoshnavazi *et al.* have reported a sandwich-type carbonate encapsulated samarium-containing silicotungstate of the formula $[(\beta-$

$\text{SiW}_9\text{O}_{34})_2(\text{H}_2\text{OSm})_3\text{CO}_3]^{13-}$, which consists of a planar triad of three lanthanide ions. Further, they also synthesized samarium-containing arseno and germanotungstate analogs; $[(\alpha\text{-AsW}_9\text{O}_{34})_2(\text{H}_2\text{OSm})_3\text{CO}_3]^{11-}$ and $[(\beta\text{-GeW}_9\text{O}_{34})_2(\text{H}_2\text{OSm})_3\text{CO}_3]^{13-}$, respectively.^[18-20] A new class of lanthanide-containing phosphotungstates $[(\text{PLn}_2\text{W}_{10}\text{O}_{38})_4(\text{W}_3\text{O}_{14})]^{30-}$ ($\text{Ln}^{\text{III}} = \text{Y}$, and Eu) was reported by Francesconi and co-workers.^[21] Later, Khosnavazi's group showed that in aqueous solution, the carbonate encapsulated samarium-containing sandwich-type $[(\alpha\text{-SiW}_9\text{O}_{34})_2(\text{H}_2\text{OSm})_3\text{CO}_3]^{13-}$ complex convert into a new class of rare-earth metal-substituted polyoxometalate of the formula $[(\text{SiW}_{10}\text{Sm}_2\text{O}_{38})_4(\text{W}_3\text{O}_8(\text{OH})_4)(\text{H}_2\text{O})_2]^{26-}$.^[22] In 2014, Hussain *et al.* have reported a series of lanthanide-containing phosphotungstates which resembles a similar structure reported by Francesconi. The structural formula of the complex is $[(\text{Ln}_2\text{PW}_{10}\text{O}_{38})_4(\text{W}_3\text{O}_8)(\text{OH})_4(\text{H}_2\text{O})_2]^{26-}$ ($\text{Ln}^{\text{III}} = \text{Sm}$, Eu , Gd , Tb , Dy , Ho , Er , Tm , Yb , and Y).^[23] Thereafter, germanotungstate analogs were reported by Hussain *et al.* in 2019.^[24] In addition with POMs, recently many other coordination complexes were also reported for its applications in the field of catalysis and magnetism.^[25-28] Henceforth, we utilized a similar strategy to obtain such isostructural lanthanide-substituted POMs by using a trilacunary Keggin-type $\text{Na}_{10}[\alpha\text{-SiW}_9\text{O}_{34}] \cdot 16\text{H}_2\text{O}$ precursor. We have changed the reaction parameters and optimized the reaction conditions to isolate a series of ten lanthanide-substituted silicotungstates of the formula $[(\text{Ln}_2\text{SiW}_{10}\text{O}_{38})_4(\text{W}_3\text{O}_8)(\text{OH})_4(\text{H}_2\text{O})_2]^{26-}$ [$\text{Ln}^{\text{III}} = \text{Sm}$ (1), Eu (2), Gd (3), Tb (4), Dy (5), Ho (6), Er (7), Tm (8), Yb (9), Y (10)]. Although Khosnavazi's group have reported the Sm complex, it was obtained as a by-product. The complexes reported here are obtained as a major product by employing a simple one-pot procedure under mild reaction conditions. We have investigated the photoluminescence property of complexes and are observed only in the case of the Sm, Eu, and Dy complexes. Moreover, we have also investigated the catalytic applications for the oxidation of thioethers. The screening of all the catalysts is performed under optimized conditions. However, we have selected $\{\text{Dy}_8\text{Si}_4\text{W}_{40}\}$ POM as the model catalyst and checked for the substrate scope only due to the high yield of this complex. Furthermore, due to the redox properties of POMs, electrochemistry of the synthesized complexes was carried out.

Results and Discussion

During the syntheses of compounds **1a-10a**, several prerequisite parameters such as pH, concentration of the solution, reaction temperature and time have to be taken care of. Herein, we have used 0.2 mmol of trilacunary Keggin-type $\text{Na}_{10}[\alpha\text{-SiW}_9\text{O}_{34}] \cdot 16\text{H}_2\text{O}$ precursor and reacted with 0.1 mmol of lanthanide nitrate salt in 0.25 M aqueous KCl solution. The reaction has been carried out at 80 °C for 1 h. The pH of the reaction mixture is found to be around 4.5. At this pH, the trilacunary Keggin-type $[\alpha\text{-SiW}_9\text{O}_{34}]^{10-}$ anion easily transforms to the dilacunary Keggin-type $[\alpha\text{-SiW}_{10}\text{O}_{36}]^{8-}$ ion. Colorless block-shaped crystals were isolated after two-three days. The isolated crystals were salt of mixed potassium and sodium with the formula $\text{K}_{11}\text{Na}_{15}[(\text{Ln}_2\text{SiW}_{10}\text{O}_{38})_4(\text{W}_3\text{O}_8)(\text{OH})_4(\text{H}_2\text{O})_2]$ [$\text{Ln}^{\text{III}} = \text{Sm}$ (1a), Eu (2a), Gd (3a), Tb (4a), Dy (5a), Ho (6a), Er (7a), Tm (8a), Yb (9a), Y (10a)]. Later, all the polyanions were characterized by various analytical techniques such as FT-IR, UV/Vis, TGA and

SC-XRD. These polyanions were further investigated for different applications such as in Catalysis, Photoluminescence, and Electrochemistry.

Structure of the polyanion

Herein, we have reported the synthesis of lanthanide-substituted silicotungstates, which are stable both in the solid-state as well as in an aqueous solution. All the compounds are structurally characterized by single crystal X-ray diffraction analysis which reveals that the nanoclusters are isostructural and crystallize in the monoclinic crystal system having space group *P-1*. The complexes **1a-10a** consist of four $[\text{SiW}_{10}\text{O}_{36}]^{8-}$ anions, eight Ln^{3+} cations, and seven extra tungsten atoms, which form a $[\text{Ln}_8\text{W}_7\text{O}_{30}]^{6+}$ network. The complexes are formed by four $[\text{SiW}_{10}\text{O}_{36}]^{8-}$ anions connected by a network of Ln-O bonds. Eight lanthanide ions and seven additional tungsten atoms in $[\text{Ln}_8\text{W}_7\text{O}_{30}]^{6+}$ network connected to the $[\text{SiW}_{10}\text{O}_{36}]^{8-}$ give rise to a complete tetrameric $[(\text{Ln}_2\text{SiW}_{10}\text{O}_{38})_4(\text{W}_3\text{O}_8)(\text{OH})_4(\text{H}_2\text{O})_2]^{26-}$ structure (Figure 1).

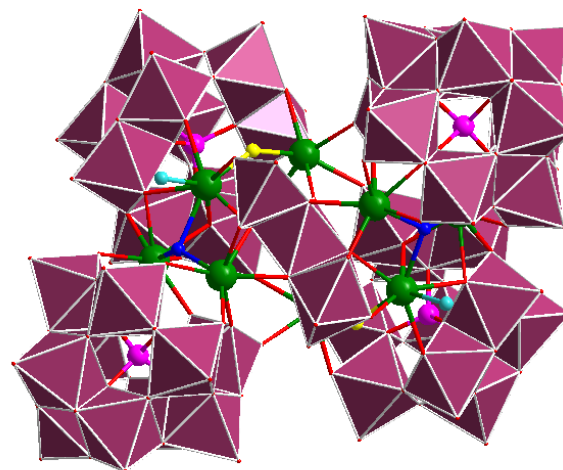


Figure 1. Polyhedral representation of the complex **1a-10a**. (Color code: dark green: lanthanide; pink: silicon; dark blue: μ_2 -OH; yellow: μ_3 -OH; aqua: terminal water molecule; plum: polyhedra).

If the extra tungsten unit is removed from the structure, then it can be seen as an assembly of two asymmetric units. Each asymmetric unit consists of four lanthanide ions and two distorted Keggin-type $[\text{SiW}_{10}\text{O}_{36}]^{8-}$ units. Each of the $[\text{SiW}_{10}\text{O}_{36}]^{8-}$ asymmetric units are substituted with two lanthanide ions (Figure 2) and these lanthanide ions are connected to Keggin-type ions via Ln-O linkages. The selected bond lengths and bond angles for Ln-O linkages are shown in Table S1 and Table S2 respectively. Bond Valence Sum (BVS) calculations were also performed for all the oxygen atoms to find out what sort of ligand they are: oxo, hydroxo or water molecules. The BVS values for the oxygen atoms bridging between lanthanide ions are found within the range of 0.95 to 1.25. This indicates that the oxygen atoms labeled as O73 and O112 are μ_2 - and μ_3 -hydroxo linkages respectively.^[29] For the terminal oxygen atom O162, the BVS value is found in the range of 0.25-0.36, suggesting it to be a water molecule. The BVS values for oxygen atoms bridging between lanthanide and tungsten atoms are found to be in the range of 1.506-1.707, which suggests that

they are oxo linkages. Henceforth, according to BVS values the polyanion has an overall charge of -26 , which is compensated with sodium and potassium cations.

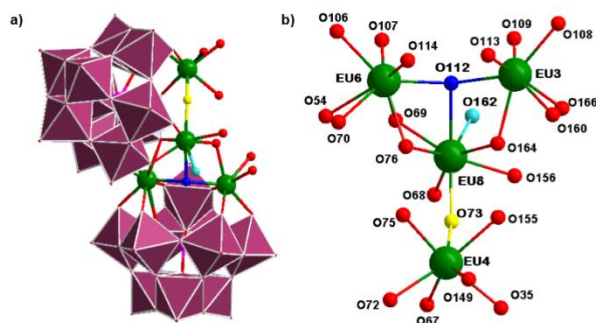


Figure 2. a) Asymmetric unit consists of two distorted Keggin-type parts $[Eu_2SiW_{10}O_{38}]^{6-}$ connected to each other by Eu–O bonds; b) Coordination environment of lanthanide ions (Color code: dark green: lanthanide; pink: silicon; dark blue: μ_3 -OH; yellow: μ_2 -OH; aqua: terminal water molecule; plum: polyhedra).

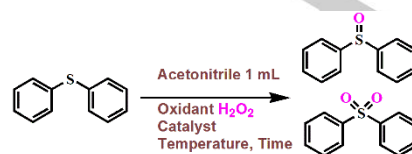
The lanthanides Eu3 and Eu4 are seven-coordinated with a capped Trigonal prismatic geometry, and the coordination sites of Eu3 are occupied by one μ_3 -OH hydroxo and six oxygen atoms connected to the parent Keggin ion. The coordination sphere of Eu4 is occupied by one μ_2 -OH and six oxygen atoms of the Keggin ion. Eu6 and Eu8 are eight-coordinated having a Square-antiprismatic geometry, and the coordination sphere of Eu8 is fulfilled with one μ_3 -OH, one terminal water molecule, and six neighboring oxygen atoms from tungsten polyhedra. Eu6 is linked with one μ_3 -OH and seven oxygen atoms from tungsten polyhedra.

Catalysis

The catalytic oxidations of organic compounds by using mild conditions have both a potential utility and wide-spread interest. The selective oxidation of thioether compounds is interesting due to the versatile application of their oxidized sulfone (RSO_2R') and sulfoxide ($RSOR'$) forms in various fields such as sulfoxidation reactions, oxido-transfer reagents, biochemistry, chemical industry, and medicinal chemistry.^[30-32] H_2O_2 has been used as an oxidant in the reaction and is also known as a “green” oxidant, as the side product of the H_2O_2 oxidation reaction is water. Polyoxometalates have been investigated as catalysts due to their versatile features such as redox properties, proton-transfer reactions, and structural variety. Here, we have utilized POM complexes as catalysts for the oxidation reaction of a standard substrate like biphenyl sulfide in the presence of H_2O_2 as the oxidant. We have investigated the catalytic behavior of the lanthanide-substituted silicotungstates $\{Dy_8Si_4W_{40}\}$ and observed that all the complexes show excellent catalytic activity (Table S4). Further, for the catalytic reactions, we have taken $\{Dy_8Si_4W_{40}\}$ as the model catalyst due to its high yield during the synthesis. The selectivity and conversion to sulfoxide ($RSOR'$) and sulfone (RSO_2R') were investigated by Gas Chromatography using the internal standard method (GC spectra Figure S12). Initially, biphenyl sulfide has been used as

a standard substrate, which is oxidized into biphenyl sulfoxide ($PhSOPh$) and biphenyl sulfone ($PhSO_2Ph$).

Table 1. Oxidation of biphenyl sulfide by using catalyst $\{Dy_8Si_4W_{40}\}$ ^[a]



Entry	Temperature (°C)	H_2O_2 (mmol)	Catalyst loading (mol %)	Conversion (%) ^[b]	Selectivity (%) ^[c]		Time (Min)
					$PhSOPh$	$PhSO_2Ph$	
1	50	4	0.14	90	20	80	40
2	50	4	0.20	99	5	95	40
3	50	4	0.27	100	0	100	40
4	40	4	0.27	100	25	75	40
5	25 (RT)	4	0.27	30	70	30	40
6	50	0	0.27	10	80	20	40
7	50	4	0.27	100	44	56	30

[a] Reaction conditions: biphenyl sulfide 0.5 mmol, oxidant H_2O_2 (30 % aqueous), 0–4 mmol, catalyst $\{Dy_8Si_4W_{40}\}$ loading 0.14–0.27 mol %, temperature 30–50 °C, 40 min, acetonitrile 1 mL. [b] Conversion based on substrate consumption and determined by GC-FID using an internal standard technique. [c] The Selectivity ($PhSOPh/PhSO_2Ph$) is determined by GC.

It was observed that the substrate was completely consumed in 40 min and produced $PhSO_2Ph$, with 100 % selectivity at 50 °C in 1 mL of acetonitrile, 0.27 mol % of the catalyst $\{Dy_8Si_4W_{40}\}$ and 4 mmol of H_2O_2 . We have also oxidized various thioethers to the corresponding oxygenated products by using H_2O_2 and $\{Dy_8Si_4W_{40}\}$ as the catalyst. When the reaction is carried out in the absence of a catalyst (Table S5, Entry 3), the conversion is only about 20 % and the selectivity of the major product ($PhSO_2Ph$) is also very low. However, as the catalyst amount is varied from 0.14–0.27 mol %, we obtain its optimized amount to be 0.27 mol %, with 100 % selectivity of sulfone (Table 1, Entry 3). Under the same conditions, we have also investigated the catalytic activity of the lanthanide salt $Dy(NO_3)_3 \cdot xH_2O$ and the trilaunary POM precursor $Na_{10}[A-\alpha-SiW_9O_{34}] \cdot 16H_2O$ in the absence of any catalyst, and the selectivity is found to be 34 % and 98 % respectively (Table S3, Entries 4 and 5). It can be observed that the silicotungstate $Na_{10}[A-\alpha-SiW_9O_{34}] \cdot 16H_2O$ precursor also shows good catalytic activity, but the amount of this precursor used is very high (1.08 mol %), and the selectivity towards the sulfone decreases upon decreasing the mol % of the precursor. Thereafter, we have performed the oxidation reaction in the absence of H_2O_2 , which results in less conversion to the desired product (Table 1, Entry 6). The small conversion of sulfone and sulfoxide was obtained due to the oxidation in presence of atmospheric oxygen.^[33] This indicates that the catalyst $\{Dy_8Si_4W_{40}\}$ shows an excellent catalytic property in the presence of H_2O_2 . Generally, POMs activate H_2O_2 by forming peroxy species. The amount of oxidant also plays an important role in the oxidation reaction, since as the oxidant amount increases the selectivity for the desired product sulfone also increases (Table S5). The optimized ratio of substrate and the oxidant is found to be 1:8 (Table S6). The reaction temperature also affects the selectivity of the biphenyl sulfone. At low

temperature, the selectivity for PhSO₂Ph is low, but increases with temperature, reaching an optimized value at 50 °C (Table 1, Entries 3, 4 and 5). All these parallel experiments indicate that the compound {Dy₈Si₄W₄₀} shows an excellent catalytic activity for the oxidation of thioethers.

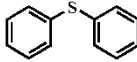
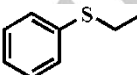
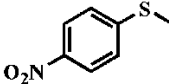
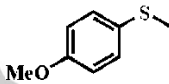
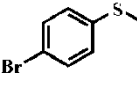
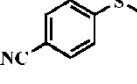
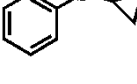
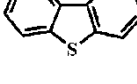

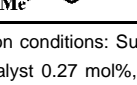
Table 2. Effect of the solvent on the reaction^[a]

Entry	Solvent	Conversion (%) ^[b]	Selectivity (%) ^[c]	
			PhSOPh	PhSO ₂ Ph
1	DMF	50	84	16
2	Toluene	14	57	43
3	H ₂ O	52	78	22
4	Acetonitrile	100	0	100
5	Acetonitrile + H ₂ O (50: 50)	50	20	80

[a] Reaction conditions: Substrate biphenyl sulfide 0.5 mmol, oxidant H₂O₂ (30 % aqueous), 4 mmol, catalyst 0.27 mol %, temperature 50 °C, 40 min, solvent 1 mL. [b] Conversion based on substrate consumption and determined by GC-FID using an internal standard technique. [c] The Selectivity (PhSOPh/PhSO₂Ph) is determined by GC.

We have also checked the catalytic performance in various solvents and it is observed that the selectivity and the conversion of the oxidation reaction are more pronounced in polar solvents as compared to non-polar ones (Table 2). Generally, this happens due to the poor solubility of the catalyst in non-polar solvents. The oxidation reaction has also been carried out in water as a green solvent, but since sulfur alkyl and aryl thioethers are not soluble in water, the catalysis reaction is not much effective. In addition, under the optimized reaction conditions, we have performed the catalysis reaction of different aromatic and alkyl thioethers. Alkyl thioethers are most reactive towards the oxidation into their corresponding sulfone due to the less steric hindrance of the alkyl group, and 100 % selectivity is obtained (Table 3, entry 9). We have also examined that the conversion is still 100 % even on increased steric hindrance, except in the few cases where the selectivity of the sulfone is decreased. Various substituents attached to the aromatic ring also affects the selectivity for the sulfone. The strong electron-withdrawing group-containing substrates, such as 4-nitrothianisol and 4-cyanothianisol, show less selectivity, as shown in Table 3 (Entries 3 and 6), due to the decrease in the electron density on the benzene ring. The electron-donating group-containing substrates, such as 4-methoxythianisol and 4-methylthianisol, as shown in Table 3 (Entries 4 and 10), show excellent selectivity which might be due to the high electron density on the sulfur atom in these substrates. We have also studied the oxidation reaction for an aromatic system such as dibenzothiophene, for which an excellent selectivity is obtained as shown in Table 3 (Entry 8). Furthermore, a recycling test was also carried out to evaluate the catalytic performance of the catalyst during the oxidation reaction of the biphenyl sulfide under optimal conditions. A hot filtration experiment was conducted, the catalyst {Dy₈Si₄W₄₀} having been removed after 10 minutes by filtration, and the reaction allowed to continue. It was observed that there is a small conversion to the product, suggesting that the reaction mechanism is heterogeneous. In this heterogeneous system, the catalyst was collected by filtration after the completion of the reaction, washed with ethyl acetate, dried, and reused in the next run.

Table 3. Selective oxidation of various alkyl and aryl derivative thioethers by using the catalyst {Dy₈Si₄W₄₀}^{a]}

Entry	Substrate	Conversion (%) ^[b]	Selectivity (%) ^[c]		Time (min)
			RSOR'	RSO ₂ R'	
1		100	0	100	40
2		100	0	100	40
3		100	20	80	60
4		100	0	100	50
5		100	0	100	30
6		100	9	91	70
7		100	0	100	30
8		100	0	100	50
9		100	0	100	30
10		100	0	100	50

[a] Reaction conditions: Substrate 0.5 mmol, oxidant H₂O₂ (30 % aqueous), 4 mmol, catalyst 0.27 mol%, temperature 50 °C, solvent 1 mL. [b] Conversion based on substrate consumption and determined by GC-FID using an internal standard technique. [c] The selectivity (RR'SO/ RR'SO₂) is determined by GC.

The recycled catalyst can be used up to five consecutive runs, and thereafter the conversion yield and selectivity decrease slightly (Figure 3). The recycled catalyst was characterized by FT-IR and it was observed that the FT-IR spectrum was similar to that of the fresh catalyst (Figure S13). The FT-IR spectrum of the recycled catalyst shows major characteristic peaks at around 998 cm^{-1} , 931 cm^{-1} , 854 cm^{-1} , 757 cm^{-1} and 700 cm^{-1} , similar to the FT-IR spectrum of the fresh catalyst. Hence, this indicates that the catalyst remains stable after five runs.

We have compared our catalyst with some reported results and concluded that $\{\text{Dy}_8\text{Si}_4\text{W}_{40}\}$ shows a better catalytic activity towards the oxidation of thioethers. Notably, our synthesized catalyst requires less time, a smaller amount of solvent, and shows a better selectivity for the sulfone. For instance, the oxidation of biphenyl sulfide (Table 3, entry 1) using $\{\text{Dy}_8\text{Si}_4\text{W}_{40}\}$ as catalyst shows 100% selectivity for sulfones, and the turnover frequency (TOF) is found to be 517.3 h^{-1} at $50\text{ }^\circ\text{C}$, which is much higher than some of the reported catalysts. In 2014, Yang *et al.* reported a catalyst, $\text{Na}_{10}\text{K}_{22}[\text{Zr}_{24}\text{O}_{22}(\text{OH})_{10}(\text{H}_2\text{O})_2(\text{W}_2\text{O}_1\text{OH})_2(\text{GeW}_9\text{O}_{34})_4(\text{GeW}_9\text{O}_{31})_2]\cdot 85\text{H}_2\text{O}$, with a turnover frequency of 22.5 h^{-1} and a selectivity for biphenyl sulfone of 73 % at $60\text{ }^\circ\text{C}$.^[34] Thereafter, in 2019, they have also reported the $(\text{NH}_4)_3\text{Na}_5\text{K}_6[\text{Zr}_4(\mu_3\text{-O})_2(\mu\text{-H})_2(\text{ox})_2(\text{SiW}_{10}\text{O}_{37})_2]\cdot 23\text{H}_2\text{O}$ catalyst with selectivity for biphenyl sulfone of 42 % and a turnover frequency of 42 h^{-1} at $60\text{ }^\circ\text{C}$.^[35]

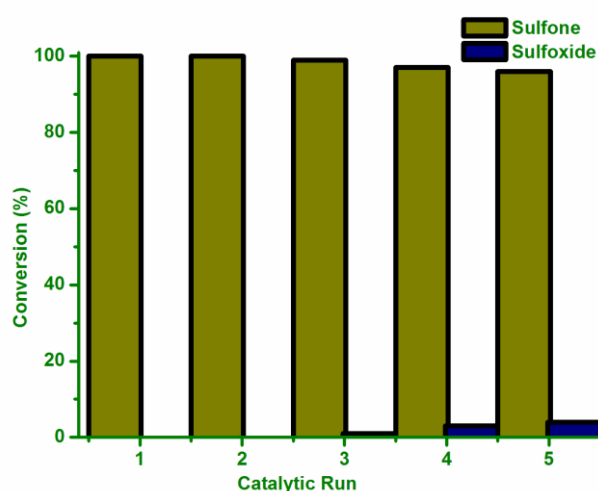


Figure 3. Catalytic runs for the oxidation reaction of thioethers under standard condition.

Electrochemistry

The electrochemical study of the compounds **1a-8a** as well as the lacunary species $\text{Na}_{10}[\text{A-}\alpha\text{-SiW}_9\text{O}_{34}]\cdot 16\text{H}_2\text{O}$ (ligand) was carried out either in lithium acetate buffer at pH 5.0 and 4.0, or in lithium sulphate buffer at pH 3.0 and 2.0. On the one hand, on a 3 hour time scale and under the present experimental conditions of cyclic voltammetry, the compounds Sm (**1a**), Eu (**2a**), Gd (**3a**), Tb (**4a**), Dy (**5a**), Er (**7a**) and Y (**9a**) showed satisfactory stability at pH 5.0 and 3.0. Meanwhile, the compounds Ho (**6a**), Tm (**8a**) and the ligand had only limited stability over time at pH 5.0 and poor stability at pH 3.0. The voltammogram of the $\text{Na}_{10}[\text{A-}\alpha\text{-SiW}_9\text{O}_{34}]\cdot 16\text{H}_2\text{O}$ compound (Figure S4) is composed of two reversible waves. The first (noted (a) in Figure S4) is multi-electronic and has a shoulder. The latter (noted (#) in Figure S4)

is in the same potential range as the first reduction wave of SiW_{11} under the same experimental conditions (CV not shown), indicating that the ligand decays and evolves into SiW_{11} . The second reduction wave (noted (b) in Figure S4) seems to indicate a reversible bi-electronic transfer. In addition, a shoulder (noted (*) in Figure S4) is observed in the reverse scan, which is not the case when the potential window is restricted to the study of just the first wave. This observation suggests that a partial degradation of the compound occurs at more negative potentials with the formation of blue derivatives.^[36,37] In addition, it should be noted that the stability of this compound over time at pH 5.0 is not marked and its decomposition kinetics increases as the pH decreases, as expected for a lacunary derivative. Its electrochemical characterisation at pH below 4.0 was not possible. At pH 5, the study of the peak current as a function of the square root of the scan rate is consistent with a diffusion-controlled system (Figure S5). The compounds **1a-10a** (except Eu (**2a**)) exhibit a similar electrochemical behaviour in cyclic voltammetry at pH 5.0 (Figure S6) as illustrated in Figure 4.

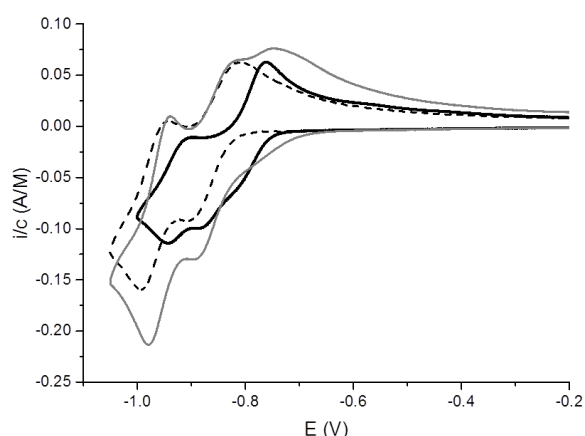


Figure 4. Cyclic voltammograms of **3a** (black and grey lines) and of the ligand (dotted line) recorded in 0.4 M $\text{LiCH}_3\text{COO}/\text{CH}_3\text{COOH}$ buffer, pH = 5.0, at $v = 0.1\text{ V/s}$. POM concentrations: $[\mathbf{3a}] = 0.195\text{ mM}$ and $[\text{ligand}] = 0.78\text{ mM}$.

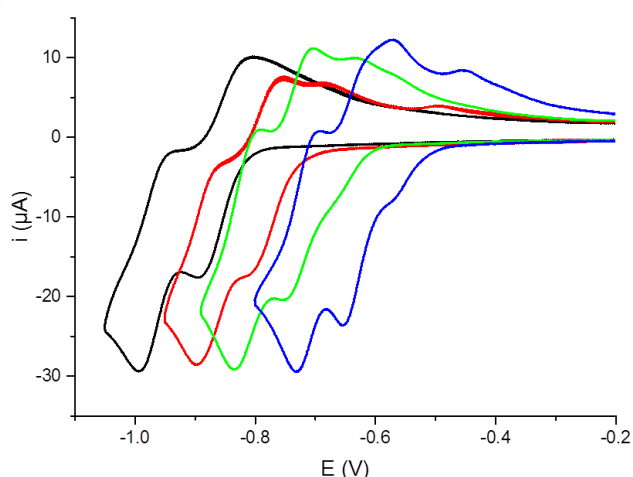


Figure 5. Cyclic voltammograms of **3a** as a function of the pH, recorded in 0.4 M $\text{LiCH}_3\text{COO}/\text{CH}_3\text{COOH}$ at pH = 5.0 (black) and 4.0 (red), and in 0.2 M $\text{Na}_2\text{SO}_4/\text{H}_2\text{SO}_4$ buffer at pH = 3.0 (green) and 2.0 (blue), at 0.1 V/s . POM concentration: $[\mathbf{3a}] = 0.195\text{ mM}$.

The cyclic voltammograms exhibit two reversible waves, the first one having an apparent redox potential ($E^{0'}$) around -860 mV, and the other one a $E^{0'}$ around -960 mV. The electrochemical signals depend on the nature of the working electrode. The best defined signals were obtained on edge-plane pyrolytic graphite (EPG) electrodes (Figure S7). The electrochemical signal of the target compounds is related to the delocalised reduction of their W^{6+} centres. Indeed, the lanthanides do not have an electrochemical signature in the potential window explored except for europium.^[6a,38] A controlled-potential coulometry study indicated that there are 16 electrons involved in the total reduction of a molecule of POM carried out at a potential corresponding to the first wave of the voltammogram. The shape of the anodic peak of the first wave depends on the vertex potential. When both waves are swept, a shoulder is visible after the anodic peak of the first wave. This shoulder is not observed when the scan is reversed right after the cathodic peak of the first wave, suggesting that an adsorption process followed by the decomposition of the compound on the electrode surface could be operative upon reaching the second wave. This hypothesis is corroborated by the observation of a peak potential difference of less than 60 mV in the second wave. The evolution of the cathodic peak current of the first wave as a function of the square root of the scan rate is linear, again being consistent with a diffusion-controlled system (Figure S8). The electrochemical behaviour as a function of the pH of the target compounds is shown in Figure 5 and summarised in Table S3. As the pH decreases, the cyclic voltammogram waves of **3a** are shifted to positive values, indicating that the electron transfer is accompanied by proton transfer. Unfortunately, it is difficult to evaluate the evolution of the apparent redox potential of each wave as a function of the pH, because the anodic peak is poorly defined for pH values below 5.0.

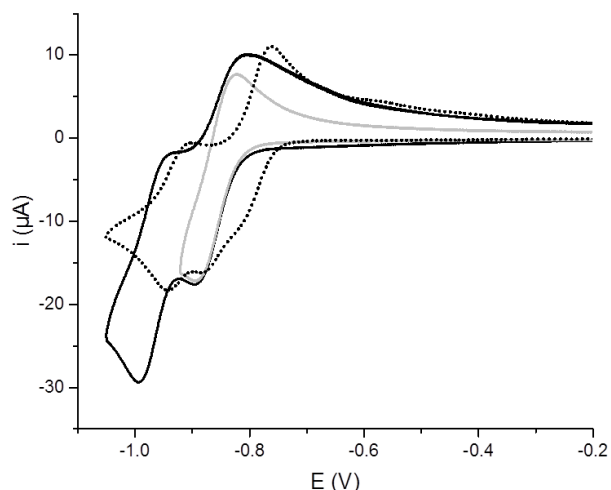


Figure 6. Cyclic voltammograms normalised with respect to the concentration of **1a** (dashed line), **2a** (grey line) and the ligand (black line), recorded in 0.4 M $\text{LiCH}_3\text{COO}/\text{CH}_3\text{COOH}$ at pH = 5.0, at $v = 0.1$ V/s.

If a rapid electron transfer is assumed at all pH values, then the peak potential difference ($\Delta E = E_{\text{pa}1} - E_{\text{pc}1}$) should be constant. Thus, plotting the evolution of $E_{\text{pc}1}$ as a function of the pH for the different compounds gives slopes close to -80 mV/pH unit. This result does not allow to draw a conclusion on the value of the ratio “number of protons exchanged/number of electrons exchanged” involved in the redox process of the first wave of the

cyclic voltammogram for each compound. The cyclic voltammogram of Eu (**2a**) shows waves of greater intensity than Sm (**1a**) (and other similar compounds, Figure S6). The first process is composite with a shoulder at -0.770 V vs SCE on the cathodic wave and a splitting on the anodic wave (Figure 6). The shoulder at -0.770 V vs SCE may be attributed to the electrochemical signal of the Eu^{3+} ions.^[7,39,40]

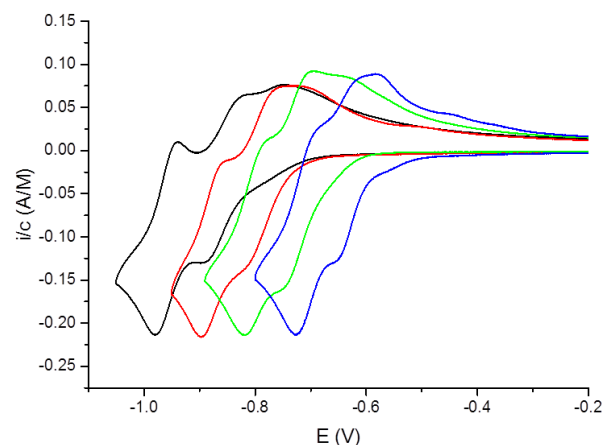


Figure 7. Cyclic voltammograms of Eu (**2a**) normalised with respect to the concentration as a function of the pH, recorded in 0.4 M $\text{LiCH}_3\text{COO}/\text{CH}_3\text{COOH}$ at pH = 5.0 (black) and 4.0 (red), and in 0.2 M $\text{Na}_2\text{SO}_4/\text{H}_2\text{SO}_4$ buffer at pH = 3.0 (green) and 2.0 (blue), at 0.1 V/s.

Indeed, in this potential range, the lacunary species does not exhibit any electrochemical signal, and the shoulder thus observed is similar to the signal observed with EuCl_3 (Figure S9). The study of the electrochemical signal as a function of the scan rate shows again that the compound is freely diffusing in solution (Figure S10). As the pH decreases, the waves in the cyclic voltammogram of Eu (**2a**) are shifted to positive values indicating that the electron transfer is accompanied by proton transfer (Figure 7). Unfortunately, it is difficult to evaluate the evolution of the apparent redox potential of each wave as a function of the pH, because the anodic peak is poorly defined for pH values below 5.0. The $E_{\text{pc}1}$ values evolve by about -77 mV per pH unit. Again, this result does not allow to draw a conclusion on the value of the ratio “number of protons exchanged/number of electrons exchanged” involved in the redox process of the first wave of the cyclic voltammogram.

Conclusion

In conclusion, we have reported a series of ten lanthanide-substituted silicotungstates of formula $\text{K}_{11}\text{Na}_{15}[(\text{Ln}_2\text{SiW}_{10}\text{O}_{38})_4(\text{W}_3\text{O}_8)(\text{OH})_4(\text{H}_2\text{O})_2]$ [$\text{Ln}^{\text{III}} = \text{Sm}$ (**1a**), Eu (**2a**), Gd (**3a**), Tb (**4a**), Dy (**5a**), Ho (**6a**), Er (**7a**), Tm (**8a**), Yb (**9a**), Y (**10a**)]. All the isolated complexes are characterized by various analytical techniques such as FT-IR, UV/Vis spectroscopy, TGA, ICP-AES, SC-XRD, and P-XRD. The single crystal X-ray diffraction reveals that all the complexes are isostructural and crystallize in the monoclinic crystal system with the space group $P-1$. The complexes **1a**, **2a** and **5a** show excellent photoluminescence properties. The complexes were used as catalysts for the oxidation of various thioethers and

show good catalytic activity. In addition, the electrochemistry properties of the complexes were also investigated.

Experimental Section

Materials and Methods

The trilaconary $\text{Na}_{10}[\text{A-}\alpha\text{-SiW}_9\text{O}_{34}] \cdot 16\text{H}_2\text{O}$ precursor was prepared according to the published literature.^[41] The FT-IR spectra of all the complexes were recorded on Perkin-Elmer BX spectrometer on KBr pellets in the range of 400-1400 cm^{-1} . Liquid UV/Vis spectroscopy was investigated on Analytic Jena Specord 250 spectrometer. Single crystal X-ray diffraction data were obtained by using an Xcalibur Oxford diffractometer operated at 50 kV and 40 mA ($\text{Mo K}\alpha_1$ radiation). Thermogravimetric analysis was performed on a DTG-60 TG/DTA instrument (Shimadzu) in the temperature range 30-400 °C. The catalytic study of the oxidation of thioethers was performed using Gas chromatography (GC Plus 2010 Shimadzu). Solid state UV/Vis spectra were recorded with a Thermo Scientific Evolution 300 spectrometer. Photoluminescence spectra were obtained with the help of a Fluorolog Horiba Jobin Yvon spectrometer. Elemental analysis was performed with an ICP-AES ARCOS instrument from M/s Spectro Germany. Electrochemical data was obtained using an Autolab PGSTAT 128N driven by a PC with the NOVA software. A one-compartment cell with a standard three electrode configuration was used for cyclic voltammetry experiments. The reference electrode was a saturated calomel electrode (SCE) and the counter electrode, a platinum plate of large surface area. The reference electrode was separated from the bulk electrolyte solution via a fritted compartment filled with the same electrolyte. The working electrode was a 3 mm diameter disk made of edge-plane pyrolytic graphite (EPG - Mersen). Before each run, the working electrode was polished with a 1 μm grain size diamond paste (DP Diamond-Struers) during 2 min and washed in an ultrasonic bath of ethanol during 2 min. Prior to each experiment, solutions were thoroughly deaerated with pure argon. A positive pressure of this gas was maintained during subsequent work. All experiments were performed at room temperature, which is controlled and fixed for the lab at 20 °C. Pure water obtained with a Milli-Q Integral 5 purification set was used throughout. All reagents were of high-purity grade and were used as purchased from Sigma Aldrich without further purification: CH_3COOH (glacial acetic acid), LiCH_3COO , Na_2SO_4 and H_2SO_4 . Powder X-ray diffraction was carried out in high resolution Rigaku X-ray diffractometer employing $\text{Cu-K}\alpha$ radiation ($\lambda = 1.5406 \text{ \AA}$) at 298 K in the range of $2\theta = 5^\circ - 30^\circ$.

Synthesis of $\text{K}_{11}\text{Na}_{15}[(\text{Sm}_2\text{SiW}_{10}\text{O}_{38})_4(\text{W}_3\text{O}_8)(\text{OH})_4(\text{H}_2\text{O})_2] \cdot 58\text{H}_2\text{O}$ (1a)

0.0889 g of $\text{Sm}(\text{NO}_3)_3 \cdot 6\text{H}_2\text{O}$ (0.2 mmol) was dissolved in 25 mL of 0.25 M potassium chloride solution. Subsequently, 0.2546 g of $\text{Na}_{10}[\text{A-}\alpha\text{-SiW}_9\text{O}_{34}] \cdot 16\text{H}_2\text{O}$ (0.1 mmol) was added to the above solution with continuous stirring and the reaction mixture was heated at 80 °C for 1 h. Thereafter, the reaction mixture was cooled at room temperature and filtered. The filtrate was left for slow evaporation in order to obtain block-shaped crystals after 2 days. The crystals were collected with a yield of 60 mg (23% based on $\text{Na}_{10}[\text{A-}\alpha\text{-SiW}_9\text{O}_{34}] \cdot 16\text{H}_2\text{O}$). FT-IR: $\bar{\nu} = 997$ (s), 936 (s), 897 (s), 853 (s) cm^{-1} . Elemental analysis (%) calcd (found): Na 2.52 (2.83), K 3.14 (4.01), W 57.68 (58.10), Si 0.82 (0.86). The number of water molecules was calculated by TGA.

Synthesis of $\text{K}_{18}\text{Na}_8[(\text{Eu}_2\text{SiW}_{10}\text{O}_{38})_4(\text{W}_3\text{O}_8)(\text{OH})_4(\text{H}_2\text{O})_2] \cdot 62\text{H}_2\text{O}$ (2a)

The above synthetic protocol procedure was followed by using $\text{Eu}(\text{NO}_3)_3 \cdot 5\text{H}_2\text{O}$ (0.0856 g, 0.2 mmol) instead of $\text{Sm}(\text{NO}_3)_3 \cdot 6\text{H}_2\text{O}$. Crystals were collected with a yield of 55 mg (21% based on $\text{Na}_{10}[\text{A-}\alpha\text{-SiW}_9\text{O}_{34}] \cdot 16\text{H}_2\text{O}$). FT-IR: $\bar{\nu} = 997$ (s), 950(s), 882 (s), 851 (s), 750 cm^{-1} . Elemental analysis (%) calcd (found): Na 1.32(1.58), K 5.06 (6.00), W

56.86 (57.60), Si 0.81 (0.90). The number of water molecules was calculated by TGA.

Synthesis of $\text{K}_{16}\text{Na}_{10}[(\text{Gd}_2\text{SiW}_{10}\text{O}_{38})_4(\text{W}_3\text{O}_8)(\text{OH})_4(\text{H}_2\text{O})_2] \cdot 59\text{H}_2\text{O}$ (3a)

The above synthetic protocol procedure was followed by using $\text{Gd}(\text{NO}_3)_3 \cdot 6\text{H}_2\text{O}$ (0.0903 g, 0.2 mmol) instead of $\text{Sm}(\text{NO}_3)_3 \cdot 6\text{H}_2\text{O}$. Crystals were collected with a yield of 57 mg (22% based on $\text{Na}_{10}[\text{A-}\alpha\text{-SiW}_9\text{O}_{34}] \cdot 16\text{H}_2\text{O}$). FT-IR: $\bar{\nu} = 999$ (s), 946(s), 885 (s), 856 (s), 745 cm^{-1} . Elemental analysis (%) calcd (found): Na 1.66 (1.80), K 4.50 (4.90), W 56.91 (58.03), Si 0.81 (0.92). The number of water molecules was calculated by TGA.

Synthesis of $\text{K}_{15}\text{Na}_{11}[(\text{Tb}_2\text{SiW}_{10}\text{O}_{38})_4(\text{W}_3\text{O}_8)(\text{OH})_4(\text{H}_2\text{O})_2] \cdot 60\text{H}_2\text{O}$ (4a)

The above synthetic protocol procedure was followed by using $\text{Tb}(\text{NO}_3)_3 \cdot 5\text{H}_2\text{O}$ (0.087 g, 0.2 mmol) instead of $\text{Sm}(\text{NO}_3)_3 \cdot 6\text{H}_2\text{O}$. Crystals were collected with a yield of 72 mg (28% based on $\text{Na}_{10}[\text{A-}\alpha\text{-SiW}_9\text{O}_{34}] \cdot 16\text{H}_2\text{O}$). FT-IR: $\bar{\nu} = 1002$ (s), 941(s), 896 (s), 855 (s), 760 cm^{-1} . Elemental analysis (%) calcd (found): Na 1.82 (1.92), K 4.22 (4.75), W 56.85 (57.20), Si 0.81 (0.87). The number of water molecules was calculated by TGA.

Synthesis of $\text{K}_{19}\text{Na}_7[(\text{Dy}_2\text{SiW}_{10}\text{O}_{38})_4(\text{W}_3\text{O}_8)(\text{OH})_4(\text{H}_2\text{O})_2] \cdot 68\text{H}_2\text{O}$ (5a)

The above synthetic protocol procedure was followed by using $\text{Dy}(\text{NO}_3)_3 \cdot \text{H}_2\text{O}$ (0.0877 g, 0.2 mmol) instead of $\text{Sm}(\text{NO}_3)_3 \cdot 6\text{H}_2\text{O}$. Crystals were collected with a yield of 77mg (30% based on $\text{Na}_{10}[\text{A-}\alpha\text{-SiW}_9\text{O}_{34}] \cdot 16\text{H}_2\text{O}$). FT-IR: $\bar{\nu} = 1000$ (s), 940 (s), 890 (s), 857 (s), 761 (m), 715 (w) cm^{-1} . Elemental analysis (%) calcd (found): Na 1.14 (1.81), K 5.25 (5.60), W 55.90 (57.10), Si 0.79 (0.87). The number of water molecules was calculated by TGA.

Synthesis of $\text{K}_{20}\text{Na}_6[(\text{Ho}_2\text{SiW}_{10}\text{O}_{38})_4(\text{W}_3\text{O}_8)(\text{OH})_4(\text{H}_2\text{O})_2] \cdot 57\text{H}_2\text{O}$ (6a)

The above synthetic protocol procedure was followed by using $\text{Ho}(\text{NO}_3)_3 \cdot 5\text{H}_2\text{O}$ (0.0882 g, 0.2 mmol) instead of $\text{Sm}(\text{NO}_3)_3 \cdot 6\text{H}_2\text{O}$. Crystals were collected with a yield of 57 mg (22% based on $\text{Na}_{10}[\text{A-}\alpha\text{-SiW}_9\text{O}_{34}] \cdot 16\text{H}_2\text{O}$). FT-IR: $\bar{\nu} = 1005$ (s), 950 (s), 880 (s), 857 (s), 755 (m) cm^{-1} . Elemental analysis (%) calcd (found): Na 0.99 (1.11), K 5.59 (6.02), W 56.55 (57.02) Si 0.80 (0.87). The number of water molecules was calculated by TGA.

Synthesis of $\text{K}_{16}\text{Na}_{10}[(\text{Er}_2\text{SiW}_{10}\text{O}_{38})_4(\text{W}_3\text{O}_8)(\text{OH})_4(\text{H}_2\text{O})_2] \cdot 60\text{H}_2\text{O}$ (7a)

The above synthetic protocol procedure was followed by using $\text{Er}(\text{NO}_3)_3 \cdot 5\text{H}_2\text{O}$ (0.0886 g, 0.2 mmol) instead of $\text{Sm}(\text{NO}_3)_3 \cdot 6\text{H}_2\text{O}$. Crystals were collected with a yield of 62 mg (24% based on $\text{Na}_{10}[\text{A-}\alpha\text{-SiW}_9\text{O}_{34}] \cdot 16\text{H}_2\text{O}$). FT-IR: $\bar{\nu} = 1002$ (s), 943 (s), 888 (s), 859 (s), 750 (w) cm^{-1} . Elemental analysis (%) calcd (found): Na 1.64 (1.89), K 4.47 (5.02), W 56.51 (58.10), Si 0.80 (0.86). The number of water molecules was calculated by TGA.

Synthesis of $\text{K}_{11}\text{Na}_{15}[(\text{Tm}_2\text{SiW}_{10}\text{O}_{38})_4(\text{W}_3\text{O}_8)(\text{OH})_4(\text{H}_2\text{O})_2] \cdot 57\text{H}_2\text{O}$ (8a)

The above synthetic protocol procedure was followed by using $\text{Tm}(\text{NO}_3)_3 \cdot 5\text{H}_2\text{O}$ (0.089 g, 0.2 mmol) instead of $\text{Sm}(\text{NO}_3)_3 \cdot 6\text{H}_2\text{O}$. Crystals were collected with a yield of 54 mg (21% based on $\text{Na}_{10}[\text{A-}\alpha\text{-SiW}_9\text{O}_{34}] \cdot 16\text{H}_2\text{O}$). FT-IR: $\bar{\nu} = 1006$ (s), 943(s), 892 (s), 857 (s), 760 (w) cm^{-1} . Elemental analysis (%) calcd (found): Na 2.49 (2.86), K 3.10 (3.48), W 56.97 (57.15), Si 0.81 (0.89). The number of water molecules was calculated by TGA.

Synthesis of $\text{K}_{11}\text{Na}_{15}[(\text{Yb}_2\text{SiW}_{10}\text{O}_{38})_4(\text{W}_3\text{O}_8)(\text{OH})_4(\text{H}_2\text{O})_2] \cdot 56\text{H}_2\text{O}$ (9a)

The above synthetic protocol procedure was followed by using $\text{Yb}(\text{NO}_3)_3 \cdot 5\text{H}_2\text{O}$ (0.0898 g, 0.2 mmol) instead of $\text{Sm}(\text{NO}_3)_3 \cdot 6\text{H}_2\text{O}$. Crystals were collected with a yield of 59 mg (23% based on $\text{Na}_{10}[\text{A}-\alpha\text{-SiW}_9\text{O}_{34}] \cdot 16\text{H}_2\text{O}$). FT-IR: $\bar{\nu} = 1008$ (s), 946 (s), 896 (s), 853 (s), 765 (w) cm^{-1} . Elemental analysis (%) calcd (found): Na 2.49 (2.60), K 3.11 (4.01), W 57.08 (58.12), Si 0.81 (0.83). The number of water molecules was calculated by TGA.

Synthesis of $\text{K}_{11}\text{Na}_{15}[(\text{Y}_2\text{SiW}_{10}\text{O}_{38})_4(\text{W}_3\text{O}_8)(\text{OH})_4(\text{H}_2\text{O})_2] \cdot 55\text{H}_2\text{O}$ (**10a**)

The above synthetic protocol procedure was followed by using $\text{Y}(\text{NO}_3)_3 \cdot 6\text{H}_2\text{O}$ (0.0766 g, 0.2 mmol) instead of $\text{Sm}(\text{NO}_3)_3 \cdot 6\text{H}_2\text{O}$. Crystals were collected with a yield of 67 mg (26% based on $\text{Na}_{10}[\text{A}-\alpha\text{-SiW}_9\text{O}_{34}] \cdot 16\text{H}_2\text{O}$). FT-IR: $\bar{\nu} = 1003$ (s), 940 (s), 895 (s), 855 (s), 760 (w) cm^{-1} . Elemental analysis (%) calcd (found): Na 1.61 (1.67), K 3.36 (3.69), W 59.89 (60.95), Si 0.85 (0.90). The number of water molecules was calculated by TGA.

X-ray crystallography

Single crystals of **1a-10a** suitable for X-ray diffraction were mounted on a capillary tube for indexing and intensity data collection at 192 K. An Xcalibur Oxford diffractometer was used which operated at 50 kV and 40 mA (Mo K_{α} , $\lambda = 0.71073$ Å, graphite monochromated).^[42] Pre-experiment, data collection and data reduction were performed with the Oxford program suite *CrysAlisPro*.^[43] An empirical adsorption correction based on symmetry equivalent reflections was applied using SCALE3 ABSPACK.^[44] The crystal structure was solved by direct methods using SHELXS-2008,^[45] which located all the heavy metal atoms (W and Ln) and enabled us to locate all the positions of other non-hydrogen atoms (O, K, Na, Si) from the difference Fourier maps. The last cycles of refinement included atomic positions, anisotropic thermal parameters for all the heavy metal atoms and isotropic thermal parameters for all other non-hydrogen (O) atoms. Some of the tungsten atoms were refined with partial occupancies and isotropic due to disorder. Due to disorder, the R-factor for some of the crystals are higher than usual but, the structure has been solved with utmost precision as possible. Some of the oxygen atoms are disordered water molecules and as a result the structure has solvent accessible voids. The data obtained are Full-matrix least squares structure refinement against $|F_o|^2$ was performed using the SHELXL-2015 package of programs.^[45] The crystal data is shown in Table 4. Further, details of the crystal structure data may be obtained from Fachinformationszentrum Karlsruhe, 76344 [Eggenstein-leopoldshafen, Germany Fax: (+49) 7247-808-666; e-mail: crysdata@fiz-karlsruhe.de], on quoting the depository number CSD 1979347 for **2a**, 2045339 for **3a**, 1979348 for **4a**, 2045340 for **5a**, 2045341 for **6a**, 1979349 for **7a**, 2045342 for **8a**, 2045343 for **9a** and 1979350 for **10a**.

FTIR Spectroscopy

FT-IR spectra of all the complexes **1a-10a** were recorded on a PerkinElmer BX spectrometer using KBr pellets. All complexes show similar spectral patterns. The finger-print region of POM ligands is in the range from 1000-400 cm^{-1} and in this region four major characteristic vibration bands (asymmetric) are obtained, which are attributed to $\nu_{\text{as}}(\text{Si}-\text{O}_a)$, terminal $\nu_{\text{as}}(\text{W}-\text{O}_t)$, corner sharing $\nu_{\text{as}}(\text{W}-\text{O}_b-\text{W})$, and edge-sharing $\nu_{\text{as}}(\text{W}-\text{O}_c-\text{W})$. The asymmetric vibration bands at 1000-1005 cm^{-1} are ascribed to $\nu_{\text{as}}(\text{Si}-\text{O}_a)$ and the bands at around 935-940 cm^{-1} are assigned to $\nu_{\text{as}}(\text{W}-\text{O}_t)$, these bands being considered as pure vibrational bands of the POM ligands. The vibration frequency in the range of 885-890 cm^{-1} is attributed to $\nu_{\text{as}}(\text{W}-\text{O}_b-\text{W})$, and the peaks at 850-855 and 800 cm^{-1} may be assigned to $\nu_{\text{as}}(\text{W}-\text{O}_c-\text{W})$ (Figure S1).

UV/Vis Spectroscopy

The liquid UV/Vis spectra of all the complexes **1a-10a** show two characteristic absorption bands: a strong band at around 240 nm and

another broad band at around 190-200 nm. The higher energy absorption band may be attributed to $\pi\text{-}\pi^*$ charge transfer transitions of terminal $\text{O}_t \rightarrow \text{W}$ bonds, and the lower energy band is due to $\rho\pi\text{-}\rho\pi^*$ charge transfer transitions of $\text{O}_{b,c} \rightarrow \text{W}$ bonds (Figure S2). We have also recorded the solid UV/Vis spectra of which the absorbance peaks are seen in three complexes (Figure S3). The complex **Sm (1a)** shows nine characteristic absorbance peaks in which two are in the UV region and the others belong to the visible range. Two absorbance peaks in the UV region are ascribed to $^6\text{H}_{5/2} \rightarrow ^2\text{D}_{1/2}$ and $^6\text{H}_{5/2} \rightarrow ^4\text{G}_{11/2}$, $^4\text{H}_{11/2}$ transitions at 370 and 390 nm respectively. Other seven absorbance peaks are assigned as $^6\text{H}_{5/2} \rightarrow ^4\text{K}_{11/2}$, $^6\text{H}_{5/2} \rightarrow ^5\text{P}_{3/2}$, $^6\text{P}_{3/2}$, $^6\text{H}_{5/2} \rightarrow ^4\text{G}_{9/2}$, $^4\text{I}_{15/2}$, $^6\text{H}_{5/2} \rightarrow ^4\text{F}_{5/2}$, $^4\text{M}_{17/2}$, $^6\text{H}_{5/2} \rightarrow ^4\text{I}_{11/2}$, $^4\text{I}_{13/2}$, $^6\text{H}_{5/2} \rightarrow ^4\text{G}_{7/2}$ and $^6\text{H}_{5/2} \rightarrow ^4\text{F}_{3/2}$ transitions at 405, 425, 445, 465, 485, 510 and 530 nm respectively.^[46,47] Five excitation peaks for the **Eu (2a)** complex are observed in the UV/Vis range which are at 362, 382, 395, 416 and 465 nm corresponding to the $^7\text{F}_0 \rightarrow ^5\text{D}_4$, $^7\text{F}_0 \rightarrow ^5\text{L}_7$, $^7\text{F}_0 \rightarrow ^5\text{L}_6$, $^7\text{F}_0 \rightarrow ^5\text{D}_3$ and $^7\text{F}_0 \rightarrow ^5\text{D}_2$ transitions respectively. The absorbance spectrum of the complex **Dy (5a)** shows a total of five absorbance peaks, three of them being very weak at 429, 454 and 479 nm. They involve excitations from the $^6\text{H}_{15/2}$ ground state to various excited states, two transitions being highly intense at 758 and 808 nm.

Photoluminescence spectroscopy

Since polyoxometalates are metal oxide nanoclusters, they have ligand to metal charge transfer properties. Initially, Yamase and co-workers investigated the photoluminescence (PL) properties of all lanthanide-substituted polyoxometalates.^[48,49] All the title polyanions were studied and some of them exhibit good photoluminescence properties on photo-excitation at room temperature. The complex ion **1a** shows four emission peaks at 565, 601, 648 and 708 nm on photo-excitation at 377 nm (Figure 8). These peaks can be assigned to the corresponding transitions $^4\text{G}_{5/2} \rightarrow ^6\text{H}_{5/2}$, $^4\text{G}_{7/2} \rightarrow ^6\text{H}_{9/2}$ and $^4\text{G}_{5/2} \rightarrow ^6\text{H}_{11/2}$ respectively. All peaks are observed in the visible region. A peak at 565 nm is known as zero-zero band and another two transitions at 648 and 708 nm are attributed to $^4\text{G}_{5/2} \rightarrow ^6\text{H}_{5/2}$ and $^4\text{G}_{7/2} \rightarrow ^6\text{H}_{9/2}$, known as magnetic dipole and electric dipole transitions, respectively.^[46-50] The photoluminescence spectra of the complex **2a** shows five emission peaks at 584, 594, 625, 656 and 704 nm. All five peaks are assigned as $^5\text{D}_0 \rightarrow ^7\text{F}_0$, $^5\text{D}_0 \rightarrow ^7\text{F}_1$, $^5\text{D}_0 \rightarrow ^7\text{F}_2$, $^5\text{D}_0 \rightarrow ^7\text{F}_3$, $^5\text{D}_0 \rightarrow ^7\text{F}_4$ respectively (Figure 9).

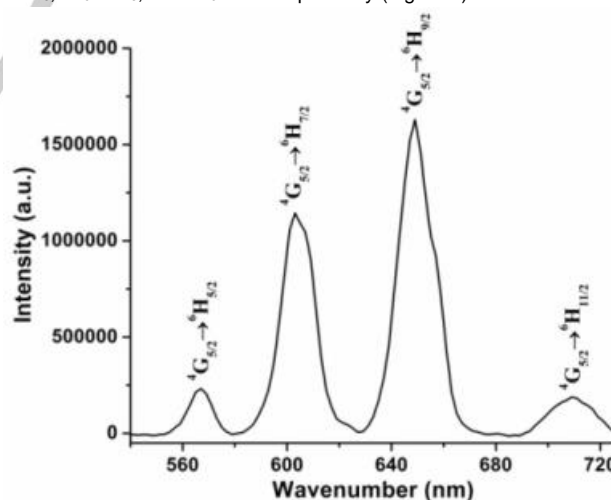


Figure 8. The photoluminescence spectrum of the complex **Sm (1a)**, excitation at 377 nm.

The transition assigned as $^5\text{D}_0 \rightarrow ^7\text{F}_1$ is magnetic dipole in nature and the intensity is independent from the environment of the Eu^{3+} ion, but directly affected by the crystal-field strength of the attached ligands. Transitions $^5\text{D}_0 \rightarrow ^7\text{F}_2$ and $^5\text{D}_0 \rightarrow ^7\text{F}_4$ are electric dipole ones, which are influenced by the chemical environment of the Eu^{3+} ion. The transition assigned as $^5\text{D}_0 \rightarrow ^7\text{F}_3$ is very weak, because it is forbidden according to the Judd-Ofelt theory.^[51,52] The PL spectra of the complex **5a** shows three characteristic emission peaks at 485, 574 and 664 which are assigned as $^4\text{F}_{3/2} \rightarrow ^6\text{H}_{15/2}$,

Table 4. Crystal data and refinement

	Eu(2a)	Gd(3a)	Tb(4a)	Dy(5a)	Ho(5a)
Empirical formula	$K_{16}Na_8Eu_8Si_4W_{43}O_{228}H_{132}$	$K_{16}Na_{10}Gd_8Si_4W_{43}O_{227}H_{126}$	$K_{15}Na_{11}Tb_8Si_4W_{43}O_{228}H_{128}$	$K_{19}Na_7Dy_8Si_4W_{43}O_{236}H_{144}$	$K_{20}Na_6Ho_8Si_4W_{43}O_{225}H_{122}$
Formula weight	13901.77	13889.79	13905.10	14142.25	13979.64
Crystal system	Triclinic	Triclinic	Triclinic	Triclinic	Triclinic
Space group	P-1	P-1	P-1	P-1	P-1
a/Å	19.6970(4)	19.6503(6)	19.6505(4)	19.7120(3)	19.6104(2)
b/Å	22.5010(5)	22.5510(7)	22.4392(4)	22.3933(4)	22.3285(2)
c/Å	27.7261(5)	27.7175(7)	27.5480(5)	27.7268(5)	27.5388(2)
α/°	85.016(2)	85.001(2)	84.717(2)	84.5880(1)	84.5980(10)
β/°	84.577(2)	84.641(2)	84.288(2)	84.5880(10)	84.2650(10)
γ/°	68.450(2)	68.218(3)	68.323(2)	68.833(2)	68.5000(10)
V/Å³	11360.1(4)	11337.5(6)	11211.9(4)	11341.3(4)	11141.66(2)
Z	1	1	2	2	1
D_c/g cm⁻³	3.798	3.898	3.952	3.888	3.870
μ/mm⁻¹	24.181	25.41	24.824	25.832	25.241
F₀₀₀	11224	11196	11546	10994	11390
Crystal size/mm³	0.08 x 0.04 x 0.02	0.08 x 0.05 x 0.02	0.07 x 0.03 x 0.02	0.10 x 0.08 x 0.03	0.10 x 0.08 x 0.03
Refins collected	147746	153475	155783	141951	177151
Indep refins	43012	42889	42498	42761	45487
R_{int}	0.1107	0.1631	0.0980	0.1649	0.0625
Goodness-of-fit on F²	1.038	1.154	1.060	1.038	1.045
R₁[I > 2σ(I)]^a	0.0808	0.1255	0.0693	0.1323	0.0505
wR₂ (all data)^b	0.2288	0.3574	0.1687	0.3176	0.1316
	Er(6a)	Tm(7a)	Yb(10a)	Y(10a)	
Empirical formula	$K_{16}Na_{10}Er_8Si_4W_{43}O_{228}H_{128}$	$K_{11}Na_{15}Tm_8Si_4W_{43}O_{225}H_{130}$	$K_{11}Na_{15}Yb_8Si_4W_{43}O_{222}H_{120}$	$K_{11}Na_{15}Y_8Si_4W_{43}O_{223}H_{126}$	
Formula weight	13987.88	13874.75	13849.52	13198.50	
Crystal system	Triclinic	Triclinic	Triclinic	Triclinic	
Space group	P-1	P-1	P-1	P-1	
a/Å	19.6576(3)	19.6577(6)	19.6283(3)	19.6091(4)	
b/Å	22.3426(3)	22.2947(6)	22.2290(3)	22.3151(5)	
c/Å	27.6670(5)	27.6328(7)	27.6410(4)	27.5576(6)	
α/°	84.7030(10)	84.669(2)	84.6040(10)	84.933(2)	
β/°	68.9950(10)	84.780(2)	84.6120(10)	84.527(2)	
γ/°	110.653(1)	69.086(3)	69.2110(10)	68.512(2)	
V/Å³	10998(3)	11241.8(6)	11201.3(3)	11150.8(4)	
Z	2	2	1	1	
D_c/g cm⁻³	3.908	3.859	3.952	3.733	
μ/mm⁻¹	25.134	25.318	24.824	24.465	
F₀₀₀	11454	11256	11264	10884	
Crystal size/mm³	0.07 x 0.03 x 0.02	0.09 x 0.07 x 0.02	0.06 x 0.05 x 0.02	0.08 x 0.06 x 0.02	
Refins collected	151119	137356	177317	155995	
Indep refins	42714	38224	45587	45566	
R_{int}	0.1026	0.1633	0.1306	0.1098	
Goodness-of-fit on F²	1.053	1.044	1.075	1.028	
R₁[I > 2σ(I)]^a	0.0708	0.1205	0.2211	0.0698	
wR₂ (all data)^b	0.2089	0.2886	0.2369	0.1840	

^[a] $R_1 = \sum |F_o| - |F_c| / \sum |F_o|$. ^[b] $wR_2 = \{\sum [w(F_o^2 - F_c^2)^2] / \sum [w(F_o^2)^2]\}^{1/2}$

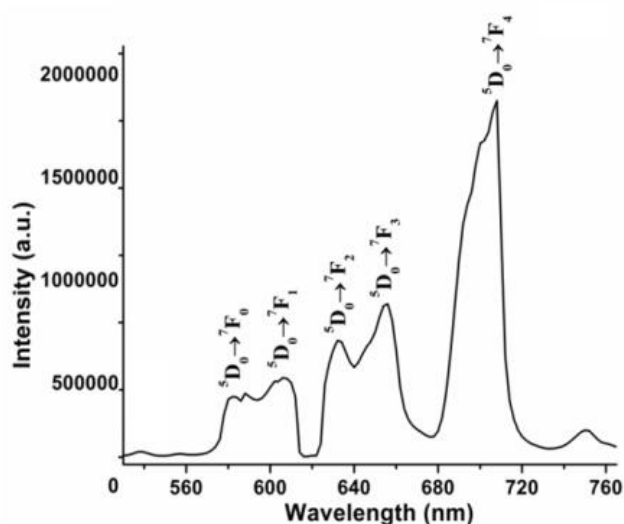


Figure 9. The photoluminescence spectrum of the complex Eu (**2a**), excitation at 460 nm.

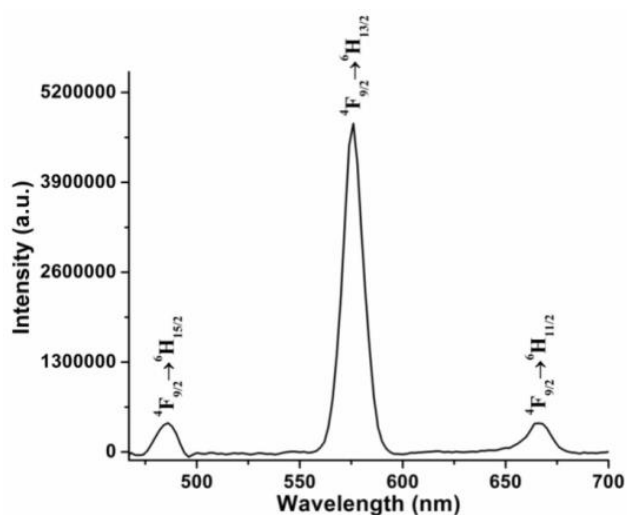


Figure 10. The photoluminescence spectrum of the complex Dy (**5a**), excitation at 370 nm.

$^4F_{9/2} \rightarrow ^6H_{13/2}$ and $^4F_{9/2} \rightarrow ^6H_{11/2}$ respectively (Figure 10). The transition corresponding to $^4F_{9/2} \rightarrow ^6H_{13/2}$ at 575 nm is related to the electric dipole environment of the Dy^{3+} ion. It has the highest intensity and is responsible for the yellow emission of the complex **5a**.^[53,54]

Experimental method for catalytic oxidation of thioethers by catalyst ($Dy_8Si_4W_{40}$)

The catalytic oxidation reactions of thioethers was performed in 25 mL round bottom flask connected to a refluxing condenser under magnetic stirring at room temperature which was heated (50 °C). The desired amount of the catalyst was added into the flask, along with 1 mL of acetonitrile solution containing thioether and oxidant. The reaction vessel was sealed and stirred into a thermostated oil bath. Reaction progress was monitored by TLC and gas chromatography. After the reaction, the vessel was cooled to room temperature and extracted with ethyl acetate for GC analysis. The thioether oxidation products (sulfoxide and sulfone) were identified with GC-MS and quantified using gas chromatography with internal standard techniques.

Thermogravimetric Analysis

The thermogravimetric analysis (TGA) of all the complexes **1a-10a** were performed in the range of 30-400 °C under inert condition (N_2 gas) at a heating rate of nitrogen gas of 5 °C/min. The TGA curves of the complexes **1a-10a** show a single step weight loss of 7.5, 7.9, 7.5, 7.6, 8.8, 7.2, 7.5, 7.3, 7.5, 7.6 % respectively, which are attributed to the loss of both lattice and coordinated water molecules (Figure S11).

Powder X-ray Diffraction

The X-ray powder diffraction patterns have been obtained for all the nanoclusters **1a-10a** which has been shown in figure S14. It has been observed that powder patterns for all the complexes perfectly matches suggesting that all ten synthesized complexes are isostructural in nature. We have also compared the powder pattern of the complex with the simulated pattern obtained from single crystal X-ray diffraction (Figure S15). Both the patterns were almost similar with slight shifting in peaks which we believe might be due to the change in crystalline material to amorphous material while drying and pressing.^[55]

Acknowledgements

F. H. thanks University of Delhi and SERB-DST project EMR/2016/002812 for the financial support. We also thank University Science Instrumentation Centre (USIC) for the instrumentation facilities and IIT Bombay for ICP-AES. I. K. and V. D. thank CSIR for fellowship. A.-L. T., I.-M.M. and P.d.O. thank the CNRS and the University Paris-Saclay for financial support.

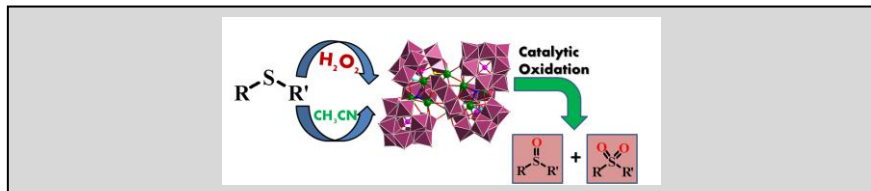
Keywords: Polyoxometalates • Lanthanide • Catalysis • Photoluminescence • Electrochemistry

- [1] a) M. T. Pope in *Heteropoly and Isopoly Oxometalates*, Springer-Verlag, Berlin, **1983**; b) M. T. Pope, A. Müller, *Angew. Chem.* **1991**, *103*, 56; *Angew. Chem. Int. Ed.* **1991**, *30*, 34.
- [2] a) M. K. Saini, R. Gupta, S. Parbhakar, S. Singh, F. Hussain, *RSC Adv.* **2014**, *4*, 38446; b) M. K. Saini, R. Gupta, S. Parbhakar, A. K. Mishra, R. Mathura, F. Hussain, *RSC Adv.* **2014**, *4*, 25357; c) F. Hussain, M. K. Saini, R. Gupta, S. Singh, *Current Catalysis* **2016**, *5*, 66.
- [3] J. M. Sumliner, H. Lv, J. Fielden, Y. V. Geletii, C. L. Hill, *Eur. J. Inorg. Chem.* **2014**, *2014*, 635.
- [4] J. T. Rhule, C. L. Hill, D. A. Judd, R. F. Schinazi, *Chem. Rev.* **1998**, *98*, 327.
- [5] P. Lei, C. Chen, J. Yang, W. Ma, J. Zhao, Li. Zang, *Environ. Sci. Technol.* **2005**, *39*, 8466.
- [6] a) R. Gupta, F. Hussain, J. N. Behera, A. M. Bossoh, I. M. Mbomekallé, P. D. Oliveira, *RSC Adv.* **2015**, *5*, 99754; b) R. Gupta, F. Hussain, M. Sadakane, C. Kato, K. Inoue, S. Nishihara, *Inorg. Chem.* **2016**, *55*, 8292; c) F. Hussain, R. W. Gable, M. Speldrich, P. Kögerler, C. Boskovic, *Chem. Commun.* **2009**, 328.
- [7] R. Gupta, M. K. Saini, F. Doungmene, P. D. Oliveira, F. Hussain, *Dalton Trans.* **2014**, *43*, 8290.
- [8] R. Gupta, I. Khan, F. Hussain, A. M. Bossoch, I. M. Mbomekallé, P. D. Oliveira, M. Sadakane, C. Kato, K. Ichihashi, K. Inoue, S. Nishihara, *Inorg. Chem.* **2017**, *56*, 8759.
- [9] R. D. Peacock, T. J. R. Weakley, *J. Chem. Soc. A* **1971**, 1836.
- [10] K. Wassermann, M. H. Dickman, M. T. Pope, *Angew. Chem.* **1997**, *109*, 1513; *Angew. Chem. Int. Ed.* **1997**, *36*, 1445.
- [11] a) L. Qu, Z. Niu, J. Liu, Y. Chen, B. Zhao, J. Peng, *Gaodeng Xuexiao Huaxue Xuebao* **1991**, *12*, 1434; b) Z. Niu, L. Qu, Y. Chen, J. Peng, J. Liu, *Yingyong Huaxue* **1992**, *9*, 46.
- [12] P. Mialane, L. Lissard, A. Mallard, J. Marrot, E. Antic Fidancev, P. Aschehoug, D. Vivien, F. Secheresse, *Inorg. Chem.* **2003**, *42*, 2102.

- [13] G. L. Xuc, J. Vaissermann, P. Gouzerh, *J. Cluster Sci.* **2002**, *13*, 409.
- [14] J. Y. Niu, J. W. Zhao, J. P. Wang, *Inorg. Chem. Commun.* **2004**, *7*, 876.
- [15] J. P. Wang, J. W. Zhao, X. Y. Duan, J. Y. Niu, *Cryst. Growth Des.* **2006**, *6*, 507.
- [16] B. Bassil, M. Dickman, I. Römer, B. Kammer, U. Kortz, *Angew. Chem.* **2007**, *119*, 6089; *Angew. Chem. Int. Ed.* **2007**, *46*, 6192.
- [17] L. B. Ni, B. Spingler, S. Weyeneth, G. R. Patzke, *Eur. J. Inorg. Chem.* **2013**, *2013*, 1681.
- [18] R. Khoshnavazi, E. Naseri, S. Tayamon, A. Ghiasi-Moaser, *Polyhedron* **2011**, *30*, 381.
- [19] R. Khoshnavazi, R. Sadeghi, L. Bahrami, *Polyhedron* **2008**, *27*, 1855.
- [20] R. Khoshnavazi, S. Gholamyan, *J. Coord. Chem.* **2010**, *63*, 3365.
- [21] R. C. Howell, F. G. Perez, W. D. Horrocks, S. Jain, A. L. Rheingold, L. C. Francesconi, *Angew. Chem.* **2001**, *113*, 4155; *Angew. Chem. Int. Ed.* **2001**, *40*, 4031.
- [22] R. Khoshnavazi, L. Bahrami, H. Davoodi, *Inorg. Chim. Acta* **2012**, *382*, 158.
- [23] R. Gupta, M. K. Saini, F. Hussain, *Eur. J. Inorg. Chem.* **2014**, *2014*, 6031.
- [24] I. Khan, R. Kaushik, R. K. Tiwari, I. Mbomekallé, P. D. Oliveira, T. Matono, H. E. Ooyama, M. Sadakane, F. Hussain, *ChemistrySelect* **2019**, *4*, 12668.
- [25] J.-X. Li, Z.-X. Du, L.-Y. Xiong, L.-L. Fu, W.-B. Bo, *Journal of Solid State Chemistry* **2021**, *293*, 121799.
- [26] J.-X. Li, Z.-X. Du, Q.-Y. Pan, L.-L. Zhang, D.-L. Liu, *Inorg. Chim. Acta* **2020**, *509*, 119677.
- [27] S. Li, P. Luo, H. Wu, C. Wei, Y. Hu, G. Qiu, *ChemCatChem* **2019**, *11*, 2978.
- [28] S. Li, Q. Mo, X. Lai, Y. Chen, C. Lin, Y. Lu, B. Liao, *Journal of Materials Research* **2019**, *34*, 3220.
- [29] I. D. Brown, D. Altermatt, *Acta Crystallogr. Sect. B* **1985**, *41*, 244.
- [30] I. Fernandez, N. Khair, *Chem. Rev.* **2003**, *103*, 3651.
- [31] J. K. Lu, X. Y. Ma, V. Singh, Y. J. Zhang, P. T. Ma, C. Zhang, J. Y. Niu, J. P. Wang, *Dalton Trans.* **2018**, *47*, 5279.
- [32] S.S. Wang, G.Y. Yang, *Chem. Rev.* **2015**, *115*, 4893.
- [33] S. Vincent, C. Lion, M. Hedayatullah, A. Challier, G. Delmas, G. Magnaud, *Phosphorus, Sulfur, and Silicon and the Related Elements* **1994**, *92*, 189.
- [34] L. Huang, S.S. Wang, J.W. Zhao, L. Cheng, G.Y. Yang, *J. Am. Chem. Soc.* **2014**, *136*, 7637.
- [35] Y. L. Wang, Z. Zhang, H.L. Li, X.Y. Li, G.Y. Yang, *Eur. J. Inorg. Chem.* **2019**, *2019*, 417.
- [36] B. Keita, L. Nadjo, *J. Electroanal. Chem. Interf. Electrochem.* **1987**, *227*, 265.
- [37] B. Keita, L. Nadjo, J. P. Haeussler, *J. Electroanal. Chem. Interf. Electrochem.* **1987**, *230*, 85.
- [38] R. Contant, G. Herve, *Rev. Inorg. Chem.* **2002**, *22*, 63.
- [39] L. Parent, P. D. Oliveira, A. L. Teillout, A. Dolbecq, M. Haouas, E. Cadot, I. M. Mbomekallé, *Inorganics* **2015**, *3*, 341.
- [40] B. Keita, L. Nadjo, *Electrochemistry of Isopoly and Heteropoly Oxometalates*, in *Encyclopedia of Electrochemistry*, **2007**, *7*, 607.
- [41] A. Tézé, G. Hervé, R. G. Finke, D. K. Lyon, *Inorg. Synth.* **1990**, *27*, 85.
- [42] Xcalibur CCD System, Oxford Diffraction Ltd., Abingdon, Oxfordshire, England, **2007**.
- [43] CrysAlis Pro software system, Version 171.32, Oxford Diffraction Ltd. Oxford, UK, **2007**.
- [44] SCALE3 ABSPACK; CrysAlisPro, Version 1.171.36.32, Oxford Diffraction Ltd., Oxford, UK, **2013**.
- [45] a) G. M. Sheldrick, *Acta Crystallogr. Sect. A: Found. Crystallogr.* **2008**, *64*, 112; b) G. M. Sheldrick, *Acta Crystallogr. Sect. C: Struct. Chem.* **2015**, *71*, 3.
- [46] L. Yang, X. Xu, L. Hao, X. Yang, J. Tang, R. Xie, *Opt. Mater.* **2011**, *33*, 1695.
- [47] X. Y. Zhao, S. X. Liu, Y. H. Ren, J. F. Cao, R. G. Cao, K. Z. Shao, *J. Solid State Chem.* **2008**, *181*, 2488.
- [48] I. Creaser, M. C. Heckel, R. J. Neitz, M. T. Pope, *Inorg. Chem.* **1993**, *32*, 1573.
- [49] a) T. Yamase, H. Naruke, *J. Chem. Soc., Dalton Trans.* **1991**, 285292; b) R. Ballardini, E. Chiorboli, V. Balzani, *Inorg. Chim. Acta* **1984**, *95*, 323.
- [50] F. S. Liu, Q. L. Liu, J. K. Liang, J. Luo, L. T. Yang, G. B. Song, Y. Zhang, L. X. Wang, J. N. Yao, G. H. Rao, *J. Lumin.* **2005**, *111*, 61.
- [51] X. Wang, Y. Guo, Y. Li, C. Hu, N. Hu, *Inorg. Chem.* **2003**, *42*, 4135.
- [52] P. Mialane, L. Lisnard, A. Mallard, J. Marrot, E. A. Fidancev, P. Aschehoug, D. Vivien, F. Sécheresse, *Inorg. Chem.* **2003**, *42*, 2102.
- [53] D. Shi, L. Chen, J. Zhao, Y. Wang, P. Ma, J. Niu, *Inorg. Chem. Commun.* **2011**, *14*, 324.
- [54] D. Zhang, C. Zhang, H. Chen, P. Ma, J. Wang, J. Niu, *Inorg. Chim. Acta* **2012**, *391*, 218.
- [55] U. B. Mioč, M. R. Todorović, M. Davidović, P. Colombari, I. Holclajtner Antunović, Heteropoly compounds—From proton conductors to biomedical agents, *Solid State Ionics* **176** (2005) 3005-3017.

Entry for the Table of Contents

Insert graphic for Table of Contents here.



Insert text for Table of Contents here. A series of ten lanthanide-substituted $\{Ln_8Si_4W_{40}\}$ nanoclusters have been synthesized possessing a potential application in the field of Catalysis for the oxidation of thioethers. The complexes were characterized by various analytical techniques. Due to the redox properties of polyoxometalates, the electrochemistry of the synthesized nanoclusters were carried out. Furthermore, the photoluminescence properties were observed in three complexes.

Institute and/or researcher Twitter usernames: ((optional))